EBioMedicine 47 (2019) 269–283

Contents lists available at ScienceDirect

EBioMedicine

journal homepage: www.ebiomedicine.com

EBioMedicine
Published by THE LANCET

Glycosylated diphyllin as a broad-spectrum antiviral agent against Zika virus

Alicia Martinez-Lopez [a], Mirjana Persaud [a], Maritza Puray Chavez [b], Hongjie Zhang [c], Lijun Rong [d], Shufeng Liu [e], Tony T. Wang [e], Stefan G. Sarafianos [b], Felipe Diaz-Griffero [a,*]

[a] Department of Microbiology and Immunology, Albert Einstein College of Medicine Bronx, NY 10461, USA
[b] Laboratory of Biochemical Pharmacology Emory University, Emory University, Atlanta, GA 30322, USA
[c] School of Chinese Medicine, Hong Kong Baptist University, 7 Baptist University Road, Kowloon Tong, Hong Kong SAR, People's Republic of China
[d] Microbiology and Immunology College of Medicine, University of Illinois at Chicago, IL 60612, USA
[e] Laboratory of Vector-borne Viral Diseases, Division of Viral Products, Center for Biologics Evaluation and Research, Food and Drug Administration, Silver Spring, MD 20903, USA

ARTICLE INFO

Article history:
Received 29 May 2019
Received in revised form 24 August 2019
Accepted 24 August 2019
Available online 6 September 2019

Keywords:
Zika
Glycosylated diphyllin
Fusion
Endosomal
pH
Ifnar1$^{-/-}$

ABSTRACT

Background: Flaviviruses such as Zika cause sporadic pandemic outbreaks worldwide. There is an urgent need for anti-Zika virus (ZIKV) drugs to prevent mother-to-child transmission of ZIKV, new infections in high-risk populations, and the infection of medical personnel in ZIKV-affected areas.
Methods: Here, we showed that the small molecule 6-deoxyglucose-diphyllin (DGP) exhibited anti-ZIKV activity both *in vitro* and *in vivo*. DGP potently blocked ZIKV infection across all human and monkey cell lines tested. DGP also displayed broad-spectrum antiviral activity against other *flaviviruses*. Remarkably, DGP prevented ZIKV-induced mortality in mice lacking the type I interferon receptor (*Ifnar1*$^{-/-}$). Cellular and virological experiments showed that DGP blocked ZIKV at a pre-fusion step or during fusion, which prevented the delivery of viral contents into the cytosol of the target cell. Mechanistic studies revealed that DGP prevented the acidification of endosomal/lysosomal compartments in target cells, thus inhibiting ZIKV fusion with cellular membranes and infection.
Findings: These investigations revealed that DGP inhibits ZIKV infection *in vitro* and *in vivo*.
Interpretation: The small molecule DGP has great potential for preclinical studies and the ability to inhibit ZIKV infection in humans.

1. Introduction

Zika virus (ZIKV) is a mosquito-borne *flavivirus* that recently caused an outbreak in humans, which resulted in fetal abnormalities such as microcephaly and neurological diseases in adults including Guillian-Barre syndrome [1–3]. ZIKV, which belongs to the *Flavivirus* genus, is a member of the Flaviviridae family along with several other important vector-borne human pathogens such as the West Nile virus (WNV), dengue virus 1 (DENV1), tick-borne encephalitis virus (TBEV), and Japanese encephalitis virus (JEV). Some of these viruses are widespread in the equatorial region, where the mosquito vectors are most prevalent [4–6]. Although ZIKV is known to be primarily transmitted through mosquito bites, some studies have shown that it can also be sexually transmitted [7–9]. For these reasons, ZIKV was recognized in 2016 as a Public Health Emergency of International Concern by the World Health Organization (WHO).

ZIKV is an enveloped virus with a 10.7-kb positive-sense, single-stranded RNA genome that encodes a polyprotein, which is post-translationally processed into three structural proteins (Capsid/C; pre-membrane/prM; and Envelope/E) and seven non-structural proteins (NS1, NS2A, NS2B, NS3, NS4A, NS4B, and NS5) [10–15]. The structural proteins protect the genome and help in virus entry into and exit from the cell, and also serve as targets for the host antibody-mediated immune response. On the other hand, the non-structural proteins are required for replication of the viral genome, processing of polyproteins, and restriction of the host innate immune response [4–6].

The study of ZIKV infection in animal models has been possible due to the availability of mice strains that are susceptible to infection. A commonly used strain is the C57BL/6 mouse that contains a knockout of the type I interferon (IFN) receptor (*Ifnar1*$^{-/-}$) [16–20]. Upon ZIKV challenge, these mice display viral infection in the central nervous system (CNS), gonads, serum, and other vital organs, which eventually leads to mortality. Other ZIKV infection models include the *Irf3*$^{-/-}$

* Corresponding author at: Albert Einstein College of Medicine, 1301 Morris Park, Price Center 501, New York, NY 10461, USA.
E-mail address: felipe.diaz-griffero@einstein.yu.edu (F. Diaz-Griffero).

https://doi.org/10.1016/j.ebiom.2019.08.060

Research in context

Evidence before this study

Zika virus is a mosquito-borne *flavivirus* that caused the 2016 outbreak in Brazil. Because Zika virus infection has been associated with neurological disorders such as Guillain-Barre syndrome and microcephaly in newborns, the recent Zika outbreak has been declared a public health emergency concern by the World Health Organization. There is an urgent need for novel antivirals with the potential to be used in the clinic. These novel antivirals are indispensable to prevent new Zika virus infections in high-risk populations, infection of medical personnel in Zika virus affected areas, and mother-to-child transmission of Zika virus.

Added value of this study

Here we discovered a new small molecule with the ability to block Zika virus infection in human cells (*in vitro*) and in mice (*in vivo*). 6-deoxyglucose-diphyllin (DGP) is a broad-spectrum antiviral that potently block infection by Zika, Dengue, Yellow fever, tick-borne encephalitis, Japanese encephalitis, West Nile and Ebola viruses. DGP targets the cellular endosomal acidification, preventing the entry of the virus into the cell consequentially inhibiting infection. Because of its effectiveness against Zika virus infection in mice, this new inhibitor shows great potential for its use in the clinics.

Implications of all the available evidence

The small molecule DGP potently inhibits Zika virus infection at very low concentrations (nM range) while its toxicity is undetectable. Furthermore, this compound effectively prevents Zika virus-induced death in mice. Altogether this evidence shows the great potential of DGP for preclinical studies.

Irf5$^{-/-}$*Irf7*$^{-/-}$, the *Stat2*$^{-/-}$ mice [18,21]; and the A129 and AG129 mice strains, which lack the IFN-α receptor or the IFN-α/β and IFN-γ receptor, respectively [22–24]. Similar results have been observed in immunocompetent mice treated with anti-IFN-αR1 monoclonal antibodies before or after ZIKV infection [25,26]. These tools have been critical for the analysis of ZIKV infection *in vivo*, as well as for the search for potential prophylactic measures and vaccine candidates.

A large number of chemical compounds with therapeutic applications have been derived from natural products, mainly from plants [27]. The natural compound 6-deoxyglucose-diphyllin (DGP), also known as Patentiflorin A, is a naphthalene-derived bioactive phytoconstituent molecule first isolated from the medicinal plant *Justicia gendarussa* [28–30]. It can be chemically synthesized by linking 6-deoxyglucose to a diphyllin molecule (Fig. 1). It was originally identified as an inhibitor of the enzyme topoisomerase II α, with potential anti-cancer properties [31,32]. Patentiflorin A has also been shown to inhibit certain human immunodeficiency virus-1 (HIV-1) strains [28].

In this study, we investigated the anti-ZIKV properties of DGP both *in vitro* and *in vivo* and explored the underlying molecular mechanism of DGP action. We showed that DGP potently inhibits infection of human cells by five different ZIKV strains in the nM range. Viral RNA imaging and quantification revealed that DGP blocks viral RNA production or an earlier stage in replication. Consistent with these results, we showed that DGP inhibits ZIKV infection during pre-fusion or fusion. Interestingly, DGP not only inhibits ZIKV infection, but also other members of the Flaviviridae family such as DENV1, JEV, TBEV, and WNV. Next, we tested the ability of DGP to prevent ZIKV infection *in vivo*.

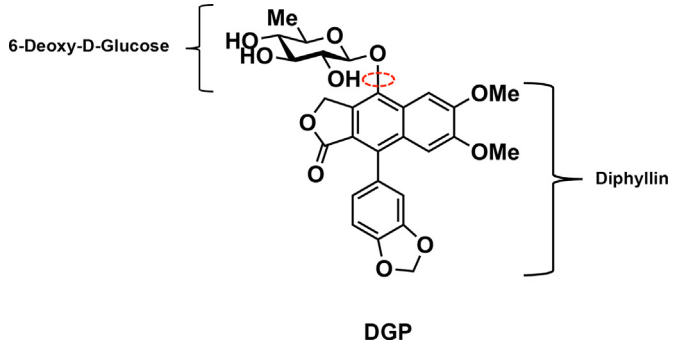

Fig. 1. Molecular structure of DGP. DGP is a naphthalene-derived bioactive phytoconstituent molecule isolated from the medicinal plant *Justicia gendarussa*, which can be chemically synthesized by linking 6-deoxyglucose to a diphyllin molecule. The bond that links 6-deoxyglucose to diphyllin is depicted with a red circle.

Remarkably, DGP (1 mg/kg) prevented ZIKV-induced mortality in *Ifnar1*$^{-/-}$ mice, showing the potential for using DGP against ZIKV infection. To understand the molecular mechanism used by DGP to block ZIKV infection, we split the DGP molecule into its smaller components and found that the active principle of DGP was diphyllin. Mechanistic studies revealed that DGP inhibited ZIKV infection by preventing acidification of endosomes.

2. Methods

2.1. Contact for reagent and resource sharing

Further information and requests for resources should be directed to and will be fulfilled by Dr. Felipe Diaz-Griffero (felipe.diaz-griffero@einstein.yu.edu).

2.2. Experimental model and subject details

2.2.1. Ethics

In vitro and *in vivo* infections were performed in a biosafety level 2 (BSL-2) room. Mice experiments were approved by the Albert Einstein College of Medicine Institutional Animal Care and Use Committee (IACUC) and performed according to the guidelines of the approved animal protocol (#20170210). Certified personnel carried out all procedures. Humane endpoint criteria in compliance with IACUC-approved scoring parameters were used to determine when the animals should be humanely euthanized.

2.2.2. Mouse studies

Mice were purchased from Jackson Laboratories and bred in a specific-pathogen-free facility at Albert Einstein College of Medicine. C57BL/6 mice that are knockout for the type I IFN receptor alpha and beta [Stock No. 32045-JAX IFN-αβR-(*Ifnar1*$^{-/-}$), Jackson Laboratories] were used for ZIKV challenges. Groups with 6 mice each (3–4 week-old, females and males) were subcutaneously injected (footpad) using 30 μL of PBS containing the indicated amount of DGP, with or without 5 PFUs of ZIKV. Mortality, symptoms, and body weight of each mouse was monitored for 15 post-challenge days.

2.2.3. Cell lines

VERO cells (ATCC CCL-81), HT1080 cells (ATCC CCL-121), and CHME3 cells (human microglia cells) were grown at 37 °C in 5% CO_2 in Dulbecco's modified Eagle's medium (DMEM) supplemented with 10% fetal calf serum (FCS), 100 IU/mL of penicillin, and 100 μg/mL of streptomycin. Cells were seeded in 24-well plates (50,000 cells/well) 24 h prior to infection with ZIKV at a multiplicity of infection (MOI) indicated for each experiment.

2.2.4. Viruses

ZIKV strain MR766 (a gift from Dr. Paul Bates), is the first described ZIKV strain that was isolated in the Zika Forest of Uganda in 1947 [33], was produced and expanded in VERO cells. ZIKV strains IbH 30656 (Human/1968/Nigeria), PRVABC59 (Human/2015/Puerto Rico), and DAK AR 41524 (Mosquito/1984/Senegal) were initially obtain from Biodefense and Emerging Infection Research Resources Repository (BEI Resources, Manassas, VA) and subsequently propagated in C6/36 cells. The Brazilian Zika strain BeH819015 (GenBank KU365778.1) virus was produced from a molecular clone generated in the Laboratory of Vector-Borne Viral Diseases (sequence available upon request) [34].

All ZIKV strains were produced and expanded in VERO cells. For viral production, VERO cells were seeded in 10-cm plates at 24 h prior to ZIKV infection. Cells were infected with ZIKV at an MOI of 10 in DMEM supplemented media with 10% FCS, 100 IU/mL of penicillin, 100 μg/mL of streptomycin, and 25 mM HEPES for 3 h. An extra 5 mL of the same media was subsequently added. The cultures were maintained for 72 h at 37 °C, after which the supernatant was collected and centrifuged for 10 min at 3000 ×*g*. ZIKV was stored in aliquots at −80 °C until further use. For virus titration, serial dilutions of ZIKV were used to challenge VERO cells; infection was determined by flow cytometry using 4G2 antibody.

Zika, Dengue 1, West Nile, Japanese encephalitis, and tick-born encephalitis viral reporter particles (ZIKV-RVP, DENV1-RVP, WNV-RVP, JEV-RVP, and TBEV-RVP) were produced by co-transfection of 293 T cells with two plasmids, the appropriate CPrME and WNV-NS-GFP, as previously shown [35]. The CPrME construct encodes the structural genes capsid (C), signal sequence, pro-membrane protein (PrM), and envelope protein (E) for each viral strain (ZIKV accession: KU312312, DENV1 accession: AHG06335.1, WNV accession: AAF20092.2, JEV accession: ADY69180.1, and TBEV accession: AAB53095.1). Sequences for ZIKV-RVP belong to the Suriname strain KU312312, which is the strain involved in a recent Brazilian outbreak [36]. To construct the CPrME for reporter viruses the following strains were used: Hypr strain for TBEV, NY-99 strain for WNV, West Pacific-74 strain for DENV1, and SX09S-01 for JEV. The genes for all the viruses were codon-optimized for mammalian cells and cloned into the pLPCX vector. The WNV-NS-GFP plasmid encodes the non-structural genes of WNV and a GFP reporter [37]. All except for the first 20 amino acids of the capsid and the last 28 amino acids of envelope of WNV genome were replaced with GFP. To generate viral particles, HEK293T cells were co-transfected with 1 μg of the CPrME constructs and 5 μg WNV-NS-GFP using polyethylimine transfection reagent at 1 mg/mL in serum-free DMEM. At 24 h post-transfection, the media was replaced with fresh DMEM and cells were maintained for an additional 24 h. The suspension was centrifuged at 3000 ×*g* for 10 min to remove cellular debris, and the supernatant containing infectious viral particles was collected. Virus stocks were stored at −80 °C and were thawed at 37 °C immediately before use.

2.3. Detection of infection by ZIKV strain MR766

The methodology used to detect ZIKV strain MR766 was previously described in [35]. In detail, cells were seeded in 24-well plates and infected with ZIKV strain MR766 at the indicated MOI for 48 h. Subsequently, cells were detached using 5 mM ethylenediaminetetraacetic acid (EDTA) in PBS, collected by centrifugation, and fixed with 1.5% paraformaldehyde in PBS for 15 min. The cells were then suspended in 0.1 M glycine for 10 min to quench the paraformaldehyde, and then washed with PBS. Cells were blocked for 30 min using 1 × Perm/Wash solution (BD Bioscience 51–2091KZ) in PBS and then incubated for 45 min in the same solution with anti-ZIKV E protein-specific monoclonal antibody 4G2, a gift of Dr. A. Brass [38]. As a control, an isotype-matched non-binding mouse IgG1 monoclonal antibody (Invitrogen Ms. IgG1) was used at approximately the same concentration on replicate samples. Afterwards, cells were washed 3 times with 1 × Perm Wash buffer and incubated with goat anti-mouse Alexa-fluor antibodies (Invitrogen, diluted 1:2000). Positive cells (ZIKV-infected) were detected using a Celesta flow cytometer (BD Biosciences). This method for quantitating infection was also used for titration of ZIKV MR766 stocks on VERO cells.

2.4. Quantitative real-time polymerase chain reaction (qRT-PCR) for the detection of ZIKV and SeV

To detect viral copies of ZIKV and Sendai Virus (SeV) by qRT-PCR, cells were seeded in 24-well plates, with or without DGP treatment, and infected with the virus at the indicated MOI for 48 h. After the incubation period, total RNA from HT1080, VERO, or CHME3 cells was isolated and purified using Trizol (Invitrogen). Briefly, after homogenizing the sample with TRIzol Reagent, chloroform is added, and the homogenate is allowed to separate into a clear upper aqueous layer (containing the RNA). RNA is then precipitated from the aqueous layer with isopropanol. Finally, the precipitated RNA is washed with 75% ethanol and then resuspended in water. For detection of ZIKV viral load in brain and spleen, 3 mice were sacrificed at 6 days post-infection and total RNA was extracted from the indicated organs. For cDNA synthesis, 1 μg of total RNA was reverse transcribed. The reaction consisted in 1 mM of deoxyribonucleotide phosphates (dNTPs), 2 μM of the specific reverse primer of ZIKV or SeV, 1× M-MULV buffer, 10 U M-MuLV RT (BioLabs), and 2 U of RNase Inhibitor, incubated for 1 h at 42 °C. followed by 20 min at 65 °C to inactivate the enzyme. For actin detection, Oligo-dT was used to reverse transcribe total RNA.

qRT-PCR was carried out using SYBR green in a 20-μL final volume reaction using a Mastercycler proS machine. The primers used to detect ZIKV were: 5′-TTGGTCATGATACTG CTGATTGC-3′-Forward (Genome Position 941–964) and 5′-CGTCGTCGTGACCAACTCTA-3′-Reverse (Genome position 1123–1103) (AY632535.2). For the detection of SeV, we used the following primers: 5′- CAGAGGAGCACAGTCTCAGTGTTC -3′-Forward (Genome position 210–233) and 5′- TCTCTGAGAGTGCT GCTTATCTGTGT −3′- Reverse (Genome position 332–307) (M30202. Genome position 210–332) [39]. For the detection of *IFN*-β: Forward 5′- ACCTCCGAAACTGAAGATCTCCTA-3′ (Genome position 644–668) and Reverse 5′-TGCTGGTTGAAGAATGCTTGA-3′ (Genome position 718–697) (NM_002176.2) and for actin detection: 5′-AACACCCCAGC CATGTACGT-′3-Forward and 5′-CGGTGAGGATCTTCATGAGGTAGT′3-Reverse. In the graphs, the data is presented as folds of induction normalized to actin.

2.5. In situ (+)-ZIKV RNA hybridization

ZIKV RNA in cultured adherent cells was probed using RNAscope reagents and protocol (Advanced Cell Diagnostics) [40], with some modifications as previously described [41]. Fixed cells on coverslips were washed twice with PBS, then incubated with 0.1% Tween-20 in PBS (PBS-T) for 10 min at room temperature (RT) and washed in PBS for 1 min. Coverslips were immobilized on glass slides, followed by protease treatment (Pretreat 3) that was diluted 1:2 in PBS and incubated on the sample in a humidified HybEZ oven at 40 °C for 15 min. The slides were washed twice with PBS for 1 min. ZIKV-specific target probe, V-ZIKA-pp-O2, for the (+) RNA (Catalog number, 464531; Advanced Cell Diagnostics) was added to the coverslip and incubated in a humidified HybEZ oven at 40 °C for 2 h. Two consecutive wash steps in 1× wash buffer (Catalog number, 310091; Advanced Cell Diagnostics) were performed on a rocking platform at RT for 2 min in every wash step after this point, and all incubations were performed in a humidified HybEZ oven at 40 °C. cDNA amplification was performed using a series of amplifiers (RNAscope; Advanced Cell Diagnostics). Amplifier hybridization 1-Fluorescent (Amp 1-FL) was added to the coverslip for 30 min, followed by Amp 2-FL hybridization for 15 min. Amp 3-FL hybridization was then added for 30 min, followed by Amp 4-FL hybridization for 15 min. Nuclei were stained with DAPI (Advanced Cell Diagnostics)

for 1 min at RT. Coverslips were washed 2 times in PBS, detached, and mounted on slides using ProLong Gold Antifade reagent (Thermo Fisher Scientific). Images were obtained using the Leica TCP SP8 inverted confocal fluorescence microscope using a 63×/1.4 oil-immersion objective. The excitation/emission bandpass wavelengths used to detect DAPI and Alexa-fluor 488 were set to 405/420–480 and 488/505–550, respectively. In order to quantify the differential drug effects on (+) ZIKV RNA, we manually acquired 25 images of each biological replicate drug treatment experiment and performed cellular analysis.

2.6. Determination of Acridine Orange fluorescence

Acridine Orange (Invitrogen) staining was performed as described previously [42,43]. Cells were stained with 1 μg/mL AO in 10% FBS DMEM for 30 min at 37 °C and then collected by trypsinization. Changes in fluorescence were measured using a Celesta flow cytometer in the PerCP-Cy5–5-A channel.

2.7. Cell viability assay

Cell viability was determined by measuring the reduction of the tetrazolium dye MTT [3-(4,5-dimethylthiazol-2-yl)-2,5-diphenyltetrazolium bromide] to its insoluble form formazan. We treated 4×10^3 cells/well in a 96-well plate with serial dilutions of the indicated drugs. Human and monkey cells were incubated with DGP, diphyllin, or 6-deoxy-D-glucose for 48 h at 37 °C. After the incubation period, 10 μL MTT solution (5 mg/mL) was added to each well for an additional 4 h at 37 °C. Finally, the media was removed and dimethyl sulfoxide was added (200 μL/well) according to the manufacturer's instructions (Invitrogen). The optical density was measured at 570 nm using a microplate reader. Experiments were performed in triplicates and standard deviations are shown. Mock-treated cells represent 100% viability.

2.8. Quantification and statistical analysis

To compare the effects of each treatment in relation to its control, all data was analyzed using the two-tailed Student's *t*-test. Differences were considered statistically significant at $P < .05$ (*), $P < .01$ (**), $P < .001$ (***), or non-significant (ns).

3. Results

3.1. The small molecule DGP blocks ZIKV infection in human and primate cell lines

We discovered the ability of DGP to inhibit ZIKV infection in human cells by serendipity. We tested the ability of DGP to block ZIKV infection in three different cell lines: African green monkey kidney epithelial cells (VERO), human fibroblast cells (HT1080), and human microglial cells (CHME3). Cells were challenged with the ZIKV strain MR766 at a multiplicity of infection (MOI) of ~1 for 48 h in the presence DGP at the indicated concentrations (Fig. 2A). ZIKV infection was measured based on the expression of the ZIKV envelope on infected cells, which was detected *via* flow cytometry in fixed/permeabilized cells using the antibody 4G2, as previously shown [35]. The use of increasing concentrations of DGP potently blocked infection of the ZIKV strain MR766 in different cell lines (Fig. 2A). Interestingly, we observed a complete block of ZIKV infection when using ~0.25–0.50 μM of DGP, thus revealing the potency of the small compound (Fig. 2A). The inhibitory concentration 50 (IC_{50}) ranged between 0.01 and 0.03 μM (Fig. 2A).

To corroborate our findings, we tested the ability of DGP to block ZIKV infection by using a ZIKV-reporter viruses (ZIKV-RVP) that express the green fluorescent protein (GFP), which are single round infection particles [35]. The production and use of ZIKV-RVP is explained in detail in the Methods section (Fig. S1). VERO, HT1080, and CHME3 cells were challenged with ZIKV-RVP at an MOI of ~0.5 for 48 h in the presence of DGP at the indicated concentrations (Fig. 2B). ZIKV-RVP infection was measured by detecting GFP expression using flow cytometry, as previously described [35]. ZIKV infection was almost completely blocked at concentrations of ~0.25–0.50 μM of DGP (Fig. 2B). The inhibitory concentration 50 (IC_{50}) ranged between 0.042 and 0.070 μM (Fig. 2A). This pattern was observed in all three cell types, regardless of the species. As a control, we used the 3-(4,5-dimethylthiazol-2-yl)-2,5-diphenyltetrazolium bromide (MTT) assay, which measures conversion of MTT to its insoluble form formazan [44,45], to show that the ZIKV inhibitory concentrations of DGP were not toxic to cells (Fig. S2). Overall, these results demonstrated that DGP is a potent inhibitor of ZIKV infection in human and primate cell lines.

In addition to the MR766 strain of ZIKV, we tested the ability of DGP to block infection of four different ZIKV strains: PRVABC59 (Puerto Rico), DAK ArD-51,254 (Senegal), IbH30656 (Nigeria), and the strain recently implicated in the 2016 outbreak, iBeH819015 (Brazilian). CHME3 cells were challenged with the different strains at the indicated concentrations of DGP, and infection was determined 48 h post-infection by measuring the percentage of infected cells by flow cytometry using 4G2 antibodies. As shown in Fig. 2C, the same inhibition pattern is observed for all of them, following a dose dependent manner, being the infection almost undetectable at 1 μM. The IC_{50} values ranged from 0.022 to 0.052 μM (Fig. 2C). These experiments showed that DGP inhibits all tested ZIKV strains.

To understand whether DGP has virucidal activity, we incubated 10^7 PFUs of ZIKV MR766 with 10, 100 or 500 μM of DGP for 1 h at 37 °C. Subsequently, the viral titer for every mixture was determined in human CHME3 cells (Fig. S3). As shown in Fig. S3, DGP did not show virucidal effect at any of the tested concentrations.

3.2. DGP blocks ZIKV infection prior to or during viral fusion

To determine the ZIKV life cycle stage at which DGP acts, we first used two approaches to measure the production of viral RNA: 1) *In situ* hybridization to image viral RNA by using fluorescent probes, and 2) qRT-PCR to quantify viral RNA. To image viral RNA, VERO cells were challenged with the ZIKV strain MR766 at an MOI of ~0.5 in the presence of 1 μM DGP, which potently blocks infection. At 48 h post-infection, cells were fixed/permeabilized and ZIKV positive-strand RNA was detected by *in situ* hybridization using a specific fluorescently labeled negative-strand probe (green). Cell nuclei were stained using 4′,6-diamidino-2-phenylindole (DAPI; blue). Twenty-five random images were captured for each treatment (Mock, ZIKV MR766, and ZIKV MR766 + DGP 1 μM) and a representative image is shown in Fig. 3A. To quantify the extent of infection, we randomly counted ~400 cells per treatment and calculated the number of infected (green) cells (Fig. 3B). Our results showed that viral RNA was not produced in the presence of DGP suggesting that DGP blocks ZIKV infection before or during viral RNA synthesis.

To corroborate these findings, we used qRT-PCR to quantify viral RNA using specific primers for the ZIKV genome (Fig. 3C). VERO and HT1080 cells were challenged with ZIKV at an MOI of 1 in the presence of DGP at the indicated concentrations (Fig. 3C). At 48 h post-infection, ZIKV RNA was quantified by qRT-PCR, and normalized to Actin. The synthesis of viral RNA was completely inhibited in the presence of increasing concentrations of DGP in both cell lines (Fig. 3C, upper panels). Inhibition of viral RNA production correlated with the inhibition of viral infection (Fig. 3C, lower panels). Altogether, these results suggested that DGP blocks ZIKV infection before or during viral RNA synthesis. However, the question of whether DGP imposes a pre- or post-fusion block to ZIKV infection remains unanswered.

To investigate whether DGP imposes a pre- or post- fusion block to ZIKV infection, we performed a time-of-drug addition experiment for DGP and compared the pattern of inhibition to that of known pre-fusion inhibitors of ZIKV infection, such as Nanchangmycin and ammonium chloride (NH_4Cl). We challenged HT1080 cells with ZIKV-RVP at

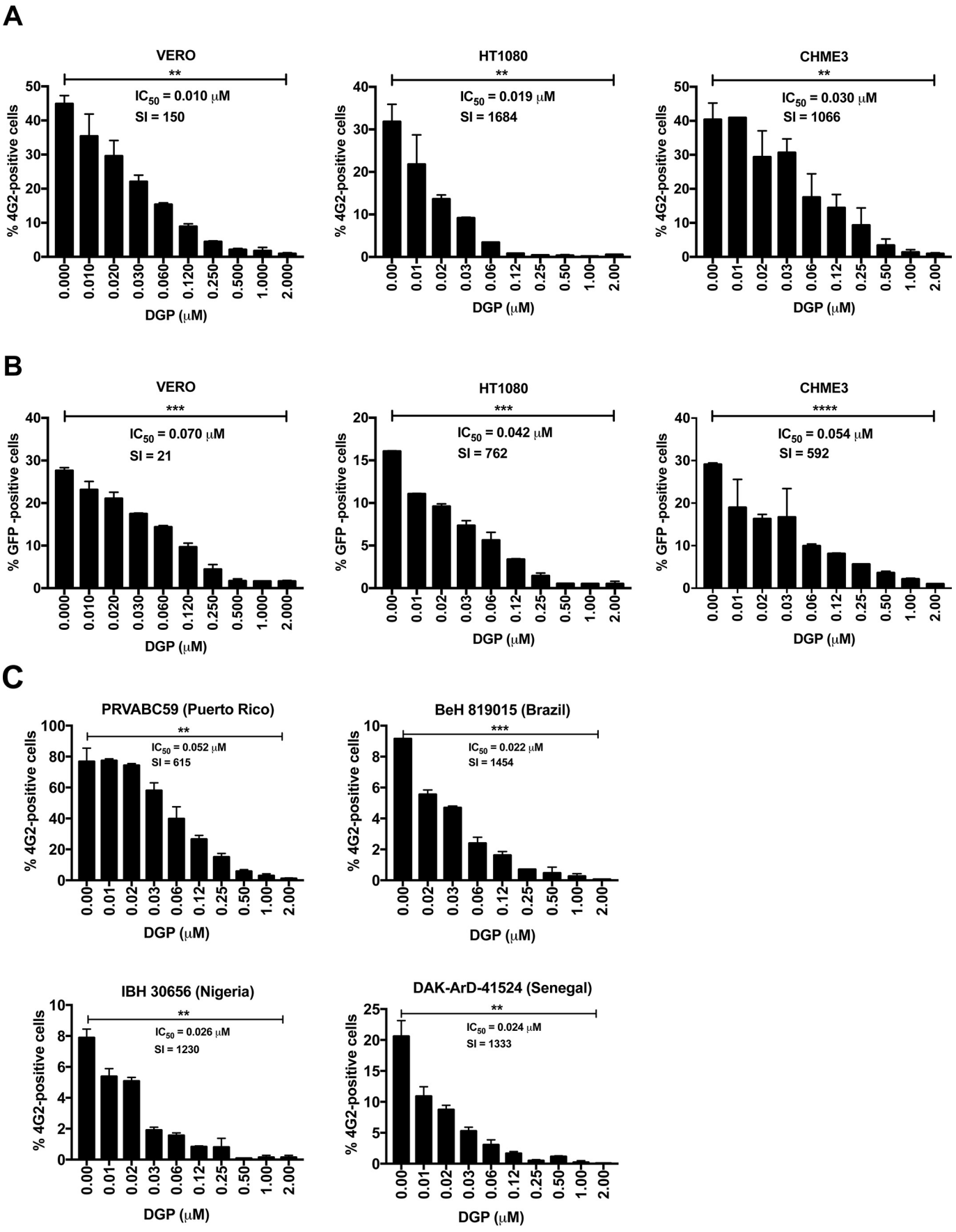
A
VERO
**
IC50 = 0.010 μM
SI = 150
% 4G2-positive cells
DGP (μM)
HT1080
**
IC50 = 0.019 μM
SI = 1684
CHME3
**
IC50 = 0.030 μM
SI = 1066
B
VERO
***
IC50 = 0.070 μM
SI = 21
% GFP -positive cells
HT1080
***
IC50 = 0.042 μM
SI = 762
CHME3
****
IC50 = 0.054 μM
SI = 592
C
PRVABC59 (Puerto Rico)
**
IC50 = 0.052 μM
SI = 615
BeH 819015 (Brazil)
***
IC50 = 0.022 μM
SI = 1454
IBH 30656 (Nigeria)
**
IC50 = 0.026 μM
SI = 1230
DAK-ArD-41524 (Senegal)
**
IC50 = 0.024 μM
SI = 1333

an MOI of ~0.5, and added 1 μM of DGP, 1 μM of Nanchangmycin, or 20 mM of NH_4Cl at the indicated time points. Infection was measured at 48 h post-infection by calculating the percentage of GFP-positive cells (Fig. 3D). We found that the inhibition of infection was stronger when the drug was added at earlier time points. Interestingly, DGP followed the same pattern of inhibition when compared with Nanchangmycin and NH_4Cl, suggesting that DGP imposes a pre-fusion block to ZIKV infection.

ZIKV infection activates the type I IFN response [46–48] *via* IFN-stimulated genes that are activated by the host after recognition of viral components [48]. If ZIKV is inhibited at a pre-fusion step, viral nucleic acids and proteins will not be exposed to the host cytosol; thus the type I IFN response will not be activated. To test whether DGP treatment prevents activation of the type I IFN response, we challenged CHME3 cells using ZIKV MR766 at an MOI of 1 in the presence of different DGP concentrations. At 48 h post-challenge, we assessed the type I IFN response by using qRT-PCR to measure *IFN-β* induction (Fig. 3E, upper panel), as previously described [49]. Consistent with the notion that DGP imposes a pre-fusion block to ZIKV infection, we found that treatment with DGP prevented the activation of the type I IFN response (Fig. 3E, upper panel). Treatment with NH_4Cl, which prevents viral fusion [35,50–57], also inhibited *IFN-β* induction. In both DGP and NH_4Cl treatments, viral infection was inhibited, as demonstrated by using the 4G2 antibody (Fig. 3E, lower panel), as previously described [35]. These results suggested that DGP inhibits ZIKV infection prior to or during the fusion step.

The *Flaviviridae* family of viruses encode a glycoprotein that is necessary to achieve fusion at the endosomal/lysosomal membranes, the step that releases viral components into the cytoplasm [55,58]. To further understand the mechanism of DGP action, we investigated the effects of DGP on viruses that do not require the fusion step at the endosomal membrane to complete their replication cycle, such as the Sendai Virus (SeV), which fuses at the plasma membrane [59–61]. To this end, we infected CHME3 cells with SeV at MOI of ~2.5, ~5 or ~10 in the presence of DGP (1 μM) or NH_4Cl and measured *IFN-β* production and viral infection. We found that DGP did not inhibit *IFN-β* production in SeV-infected cells (Fig. 3F, upper panel). Consistently, DGP treatment did not inhibit SeV infection (Fig. 3F, lower panel). Interestingly, SeV showed increased infection after DGP or NH_4Cl treatment (Fig. 3F, lower panel), which resulted in higher induction of *IFN-β* compared with the control cells (Fig. 3F, upper panel). Our results showed that DGP does not inhibit SeV infection or the resultant induction of the type I IFN response. A possible explanation for this phenomenon is that a fraction of SeV in any given infection is endocytosed and degraded by the cell; however, when lysosomotropic agents (compounds that prevent the acidification of endosomes such as DGP or NH_4Cl) are used, the degradation of SeV decreases and there is more intact virus, which results in an increased infection.

Overall, these results are in agreement with the notion that DGP blocks ZIKV infection at a pre-fusion step or during fusion at the endosomal membrane.

3.3. DGP inhibits the infectivity of other flaviviruses

Our findings have demonstrated that DGP is a potent inhibitor of ZIKV infection. Next, we tested whether DGP inhibits other Flaviviridae viruses. For this purpose, we used reporter viral particles (RVPs) expressing GFP as a reporter of infection, and containing the envelope of: DENV1, TBEV, WNV, or JEV. We also included RVPs of the Ebola virus (EBV), which belongs to the Filoviridae family, in our analysis. VERO cells were challenged with the indicated RVPs in the presence of increasing concentrations of DGP (Fig. 4). At 48 h post-challenge, infection was determined by using flow cytometry to measure the percentage of GFP-positive cells. We found that DGP showed dose-dependent inhibitory activity against all the RVPs tested. As control, cells were infected with the RVPs in the presence of 20 mM of NH_4Cl, which inhibited infection of all the tested RVPs (Fig. 4). DGP-mediated inhibition of RVP-infection was comparable to that mediated by NH_4Cl. These results showed that DGP exerts antiviral activity against different *flaviviruses*, demonstrating its potential use as a broad-spectrum antiviral agent.

3.4. DGP prevents ZIKV-induced mortality in type I interferon receptor knockout mice (*Ifnar1*$^{-/-}$)

Next, we tested the antiviral activity of DGP *in vivo* by using the mouse model C57BL/6 *Ifnar1*$^{-/-}$ [16–19], which is a knockout mouse for the type I IFN receptor α and β. To this end, we inoculated the footpad of *Ifnar1*$^{-/-}$ mice using 5 plaque forming units (PFUs) of the ZIKV strain MR766, which provides a lethal amount of virus, in conjunction with DGP. Mice that were 3–4 week-old were divided in groups (6 mice/group) and injected with the following mixtures: phosphate-buffered saline (PBS; Mock-infected), ZIKV, ZIKV +0.1 mg/kg of DGP, or ZIKV +0.2 mg/kg of DGP (Fig. 5A). Body weight and virus-induced symptoms were monitored daily in the mice for 15 days post-challenge (Fig. 5B). The group inoculated with ZIKV showed a rapid decrease in body weight, and succumbed to viral infection at day 8 post-challenge, as shown by the Kaplan-Meier plot (Fig. 5A and B); this group displayed the following phenotypes: limb paralysis, lethargic behavior, tremors, and weight loss. The group that was challenged with ZIKV +0.1 mg/kg of DGP showed similar symptoms and succumbed to viral infection at day 10 post-challenge. However, the group injected with ZIKV +0.2 mg/kg of DGP showed a delay in the appearance of symptoms when compared with the ZIKV group, and some mice survived until day 14 (Fig. 5A and B). These results indicated that DGP delayed the appearance of symptoms and delayed ZIKV-induced mortality by a few days compared with control mice.

To test whether increasing DGP concentrations increased survival in ZIKV-infected mice, three groups (6 mice/group) were injected with the following mixtures: PBS + 1 mg/kg of DGP, ZIKV, or ZIKV +1 mg/kg of DGP (Fig. 5C and D). The weight and virus-induced symptoms were monitored daily in the mice for 15 post-challenge days. As previously observed, the group inoculated with ZIKV showed a rapid decrease in body weight, and succumbed to viral infection 7–9 days post-challenge, as shown by the Kaplan-Meier plot (Fig. 5C). In contrast, all six mice in the group challenged with ZIKV +1 mg/kg of DGP survived for the length of the experiment (Fig. 5C). Two independent experiments are shown (Experiment #1 and #2). Although in experiment#1 the group injected with ZIKV +1 mg/kg of DGP showed lower body weight when compared to the group that was injected PBS + 1 mg/kg of DGP (Fig. 5D), the group injected with ZIKV +1 mg/kg of DGP did not show any obvious disease symptoms during the course of both experiments. These results demonstrated that DGP effectively inhibits ZIKV infection *in vivo* when co-injected with the virus suggesting that DGP could potentially be used to prevent or treat ZIKV infection *in vivo.*

Next we investigated whether DGP affects viral replication in the brain and spleen in mice that was challenged with ZIKV in conjunction with DGP. To this end, we determined viral loads by qRT-PCR using

Fig. 2. DGP inhibits ZIKV infection of HT1080, VERO, and CHME3 cells. HT1080, VERO, and CHME3 cells were challenged with ZIKV-MR766 (A) or ZIKV-RVPs (B) at an MOI of ~1 in conjunction with increasing concentrations of DGP. At 48 h post-challenge, infection was determined by measuring the percentage of 4G2-positive and GFP-positive cells for ZIKV-MR766 and ZIKV-RVPs infections, respectively. (C) CHME3 cells were challenged with ZIKV PRVABC59, ZIKV iBeH819015, ZIKV IbH3065, and ZIKV DAK ArD-51,254 at an MOI of 1, 0.2, 0.2 and 0.5, respectively. 48 h post-challenge, infection was determined by measuring the percentage of 4G2-positive cells. The IC_{50} and selectivity index (SI) values are shown for each of the dose-dependent curve. The SI was calculated by the ratio of CC_{50} to IC_{50}. Experiments were repeated at least three times and results of a representative experiment are shown. Bars represent the Mean ± SD. $P < .05$ (*), $P < .01$ (**), $P < .001$ (***), or not significant (ns), using two-tailed Student's *t*-test are shown.

A

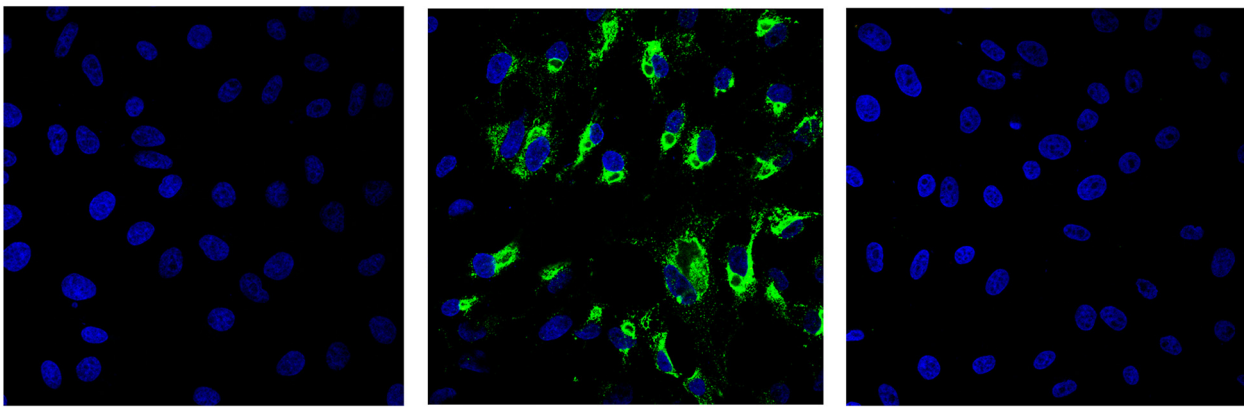

B

	Cells (Blue)	Infected cells (Green)	% Infected cells
Mock	400	0	0
ZIKV MR766	400	153	38.27
ZIKV MR766 + DGP (1 μM)	400	12	3.05

C

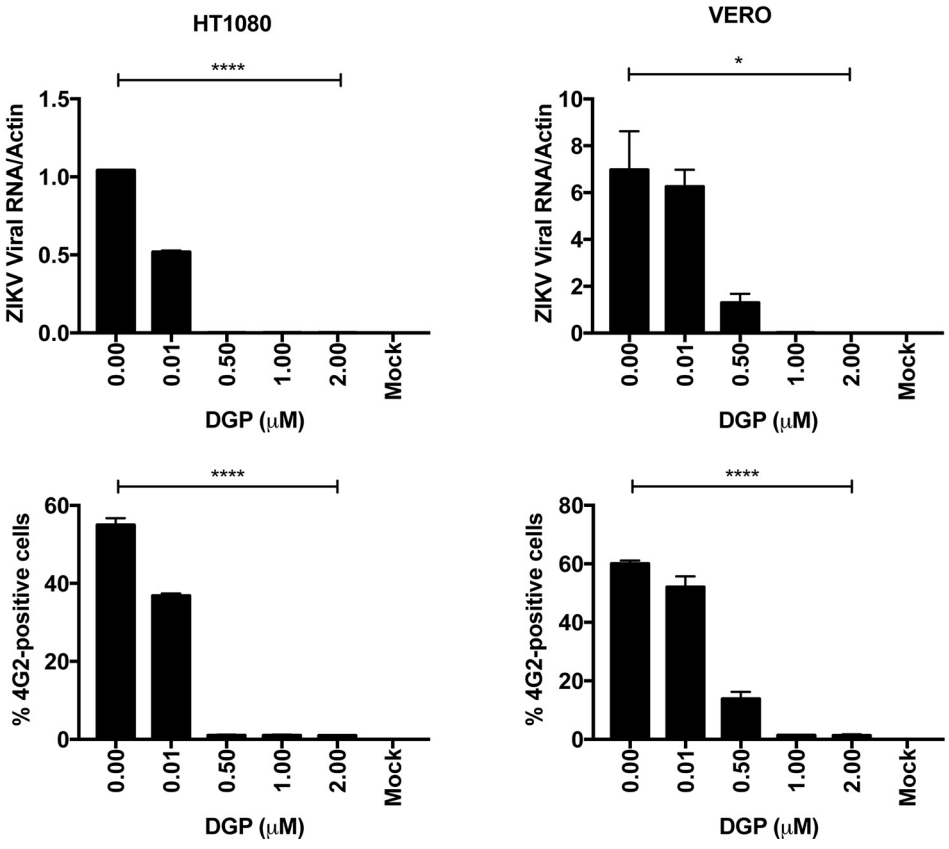

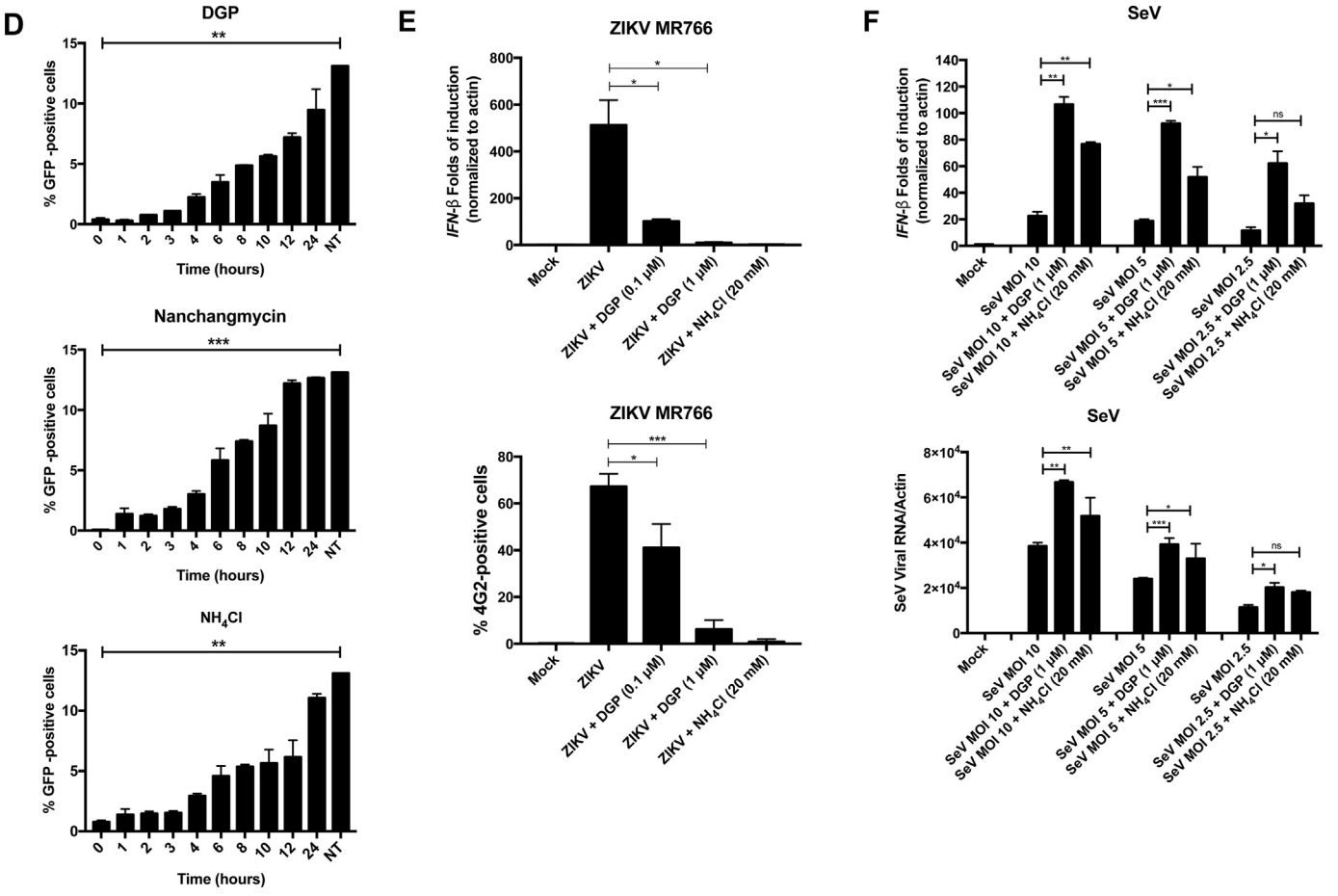

Fig. 3. DGP blocks ZIKV MR766 during fusion or at a pre-fusion step. (A) Detection of ZIKV RNA during infection by *in situ* hybridization. VERO cells were infected with ZIKV at an MOI of 0.5 in the presence of DGP. At 48 h post-challenge, cells were fixed/permeabilized and stained for the detection of positive single-stranded RNA ZIKV molecules (green). Cell nuclei were counterstained using DAPI (blue). Images were obtained using a Leica TCP SP8 inverted confocal fluorescence microscope using the 63×/1.4 oil-immersion objective. (B) The percentage of cells containing ZIKV-positive single-strand RNA (green) was determined by counting 400 DAPI-positive (blue) cells. The fraction of infected cells per treatment is shown. (C) ZIKV RNA levels were measured using qRT-PCR. HT1080 and VERO cells were challenged by ZIKV MR766 at an MOI of 1 in the presence of DGP. At 48 h post-challenge, cells were lysed and total RNA was extracted using trizol. Total RNA was used to determine the levels of ZIKV RNA by qRT-PCR using specific primers against ZIKA. ZIKA viral RNA levels were normalized to actin (upper panels). In parallel, similar infections were used to determine infectivity *via* flow cytometry using anti-4G2 antibodies (lower panels). Experiments were performed at least three times, and results of a representative experiment are shown. (D) Kinetics of ZIKV entry. ZIKV-RVPs were pre-bound to HT1080 cells at 4 °C for 1 h. Infection was initiated by raising the temperature to 37 °C. At the indicated time points, cells were treated with 1 μM of DGP, 1 μM of Nanchangmycin, or 20 mM ammonium chloride(NH_4Cl). 48 h post-challenge, infection was determined by measuring the percentage of GFP-positive cells. Experiments were repeated at least three times and results of a representative experiment are shown. NT, not treated. (E) CHME3 cells were infected with ZIKV MR766 at an MOI of 1 in the presence of the indicated concentrations of DGP. At 48 h post-challenge, the levels of *IFN*-β were measured using qRT-PCR. The levels of *IFN*-β were normalized to actin (upper panel). In parallel, ZIKV infection was measured by determining the percentage of infected cells using anti-4G2 antibodies (lower panel). Experiments were repeated at least three times and results of a representative experiment are shown. (F) CHME3 cells were infected with Sendai virus (SeV) at an MOI of ~2.5, ~5 or ~10 in the presence of 1 μM DGP. At 48 h post-infection, the levels of *IFN*-β were quantified by qRT-PCR and normalized to actin (upper panel). In parallel, SeV infection was measured by qRT-PCR using specific primers against SeV (lower panel). Experiments were repeated at least three times and results of a representative experiment are shown. Bars represent the Mean ± SD. $P < .05$ (*), $P < .01$ (**), $P < .001$ (***), or not significant (ns), using two-tailed Student's *t*-test are shown.

specific primers against the ZIKV genome six days post-challenge. As shown in Fig. 5E, the use of 1 mg/kg of DGP completely inhibits the occurrence of viral replication in the brain that correlates with protection against ZIKV-induced death; however, a small amount of viral replication can be detected in the spleen, which may not be sufficient to cause death. These experiments suggested that DGP is preventing the virus to reach the brain, hence conferring a higher rate of survival.

3.5. The active principle of DGP is diphyllin

DGP is a diphyllin derivative in which the hydroxyl group is substituted with 6-deoxy-D-glucose (6DG) (Figs. 1 and 6A). To understand the active component of DGP that contributes to its antiviral activity, we tested the individual abilities of diphyllin and 6DG to inhibit ZIKV infection (Fig. 6B and C). To this end, we challenged human HT1080 and CHME3 cells with ZIKV (MOI of 1) in the presence of increasing concentrations of the indicated drug (Fig. 6B and C), and monitored infection for 48 h post-challenge by measuring the percentage of 4G2-positive cells. We found that diphyllin blocked ZIKV infection in HT1080 cells with an IC_{50} of ~0.06 μM, whereas the IC_{50} of DGP was ~0.02 μM (Fig. 6B). Similarly, for CHME3 cells (Fig. 6C), the IC_{50} for Diphyllin was ~0.21 μM, whereas the IC_{50} of DGP was ~0.04 μM. These results indicated that diphyllin is the active component of DGP that contributes to its antiviral activity. By contrast, 6DG did not show antiviral activity against ZIKV infection (Fig. 6B and C). Interestingly, DGP was ~2–4-fold more potent than diphyllin, which suggested that the addition of 6DG to diphyllin contributes to increased antiviral activity. As control, we used the MTT assay test to ensure that the concentrations of diphyllin and DGP required to inhibit ZIKV infection were not toxic to human or monkey cells (Fig. S2). Our results suggested that the active component of DGP is diphyllin, and that 6DG contributes to the potency of DGP.

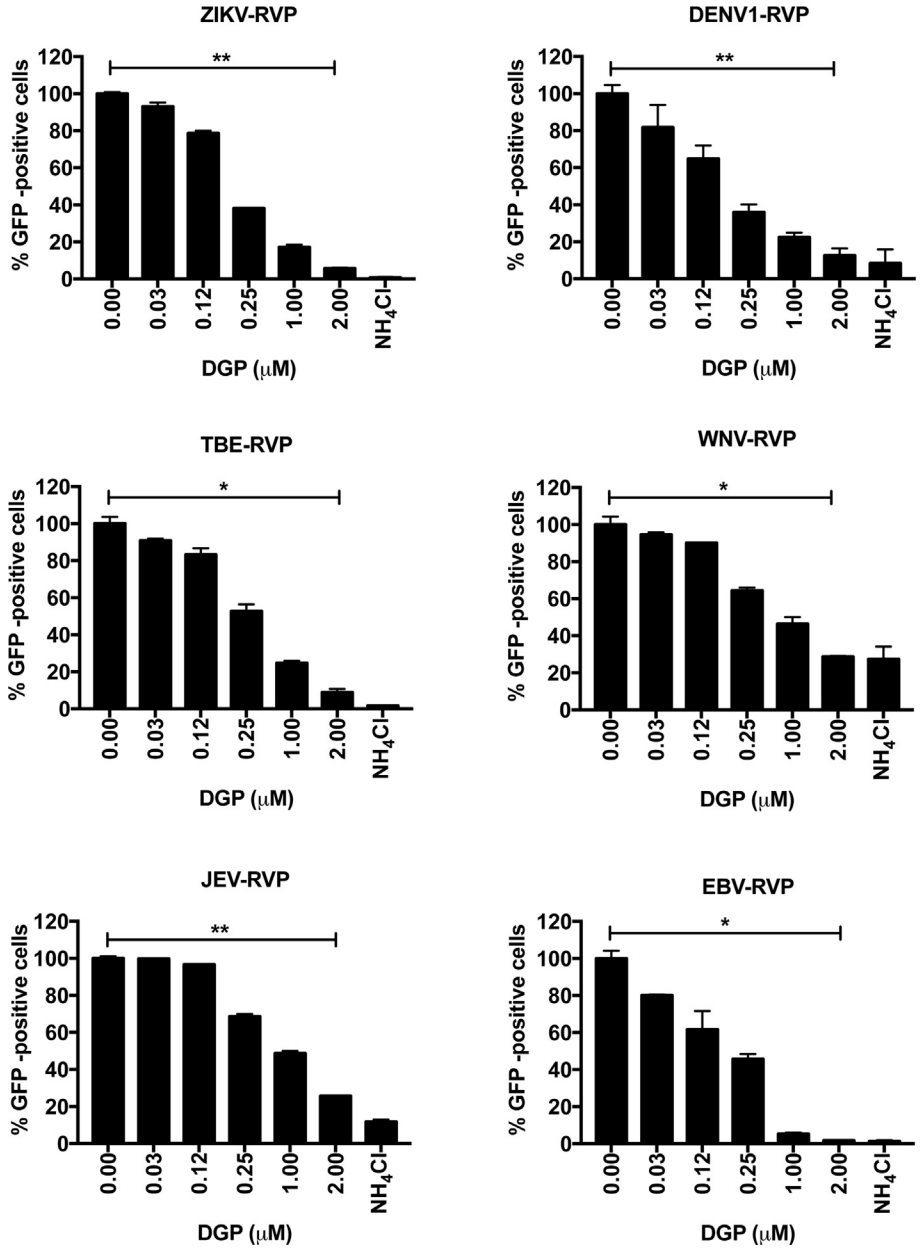

Fig. 4. DGP blocks infectivity of other Flaviviruses. DENV1, JEV, TBEV, WNV, and EBV reporter viral particles expressing GFP were used to challenge VERO cells in the presence of increasing concentrations of DGP. At 48 h post-challenge, infection was determined by measuring the percentage of GFP-positive cells using a flow cytometer. Infection values were normalized to the values of infection without DGP. Experiments were repeated at least three times and results of a representative experiment are shown. Bars represent the Mean ± SD. P < .05 (*), P < .01 (**), P < .001 (***), or not significant (ns), using two-tailed Student's *t*-test are shown.

3.6. DGP inhibits ZIKV fusion by preventing acidification of endosomes

Previous studies have shown that diphyllin affects the expression of vacuolar-ATPase, resulting in changes to the pH gradients in cells [62,63]. Vacuolar-ATPases are cellular proton pumps that are crucial for processes that maintain pH gradients in the cell, such as the acidification of endosomes [64]. Because DGP blocks ZIKV infection at a pre-fusion step, we decided to test whether DGP inhibited ZIKV infection by preventing the acidification of endosomes and lysosomes. For this purpose, we used Acridine Orange (AO), a cell-permeable fluorescent dye marker that accumulates in low pH compartments such as endosomes and lysosomes [42]. Within these acidic cellular compartments, AO displays orange fluorescence [42,65]; however, this orange fluorescence dramatically decreases in the presence of compounds that prevent acidification of endosomes, such as the vacuolar ATPase inhibitor Bafilomycin A1 [42,65].

To test whether DGP prevents endosomal/lysosomal acidification, we pre-incubated HT1080 cells with 2 μM, 1 μM, or 0.1 μM of DGP for 4 h and then stained cells using 1 μg/mL of AO (Fig. 7). Changes in fluorescence were measured using a Celesta flow cytometer in the PerCP-Cy5–5-A channel. As shown in Fig. 7, increasing DGP concentrations resulted in decreased AO fluorescence in HT1080 cells, suggesting that DGP prevents the acidification of endosomal and lysosomal compartments. As positive controls, we used Bafilomycin A1 and NH_4Cl, both of which prevent endosomal and lysosomal acidification [65]. Consistent with our hypothesis, DGP and Bafilomycin A1 treatments showed similar decreases in AO fluorescence (Fig. 7A and B). Diphyllin also prevented the acidification of endosomes and lysosomes albeit to a lower extent when compared with DGP (Fig. 7). Consistent with our previous results (Fig. 6), 6DG did not prevent the acidification of endosomes and lysosomes (Fig. 7). The loss of red fluorescence intensity compared with stained non-treated control cells is shown as mean

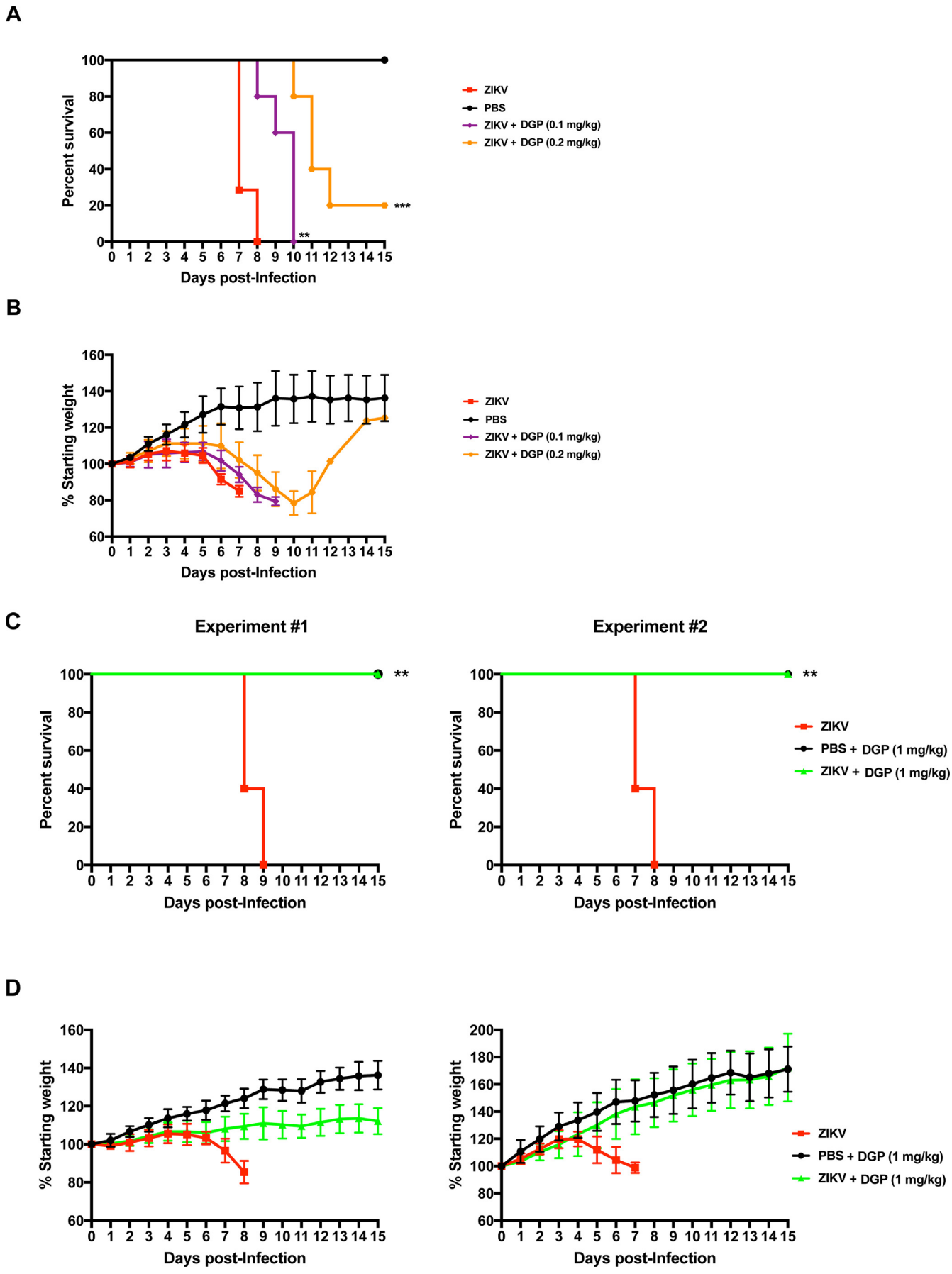
A
Percent survival
Days post-Infection
ZIKV
PBS
ZIKV + DGP (0.1 mg/kg)
ZIKV + DGP (0.2 mg/kg)
**
***
B
% Starting weight
Days post-Infection
ZIKV
PBS
ZIKV + DGP (0.1 mg/kg)
ZIKV + DGP (0.2 mg/kg)
C
Experiment #1
Experiment #2
Percent survival
Days post-Infection
**
ZIKV
PBS + DGP (1 mg/kg)
ZIKV + DGP (1 mg/kg)
D
% Starting weight
Days post-Infection
ZIKV
PBS + DGP (1 mg/kg)
ZIKV + DGP (1 mg/kg)

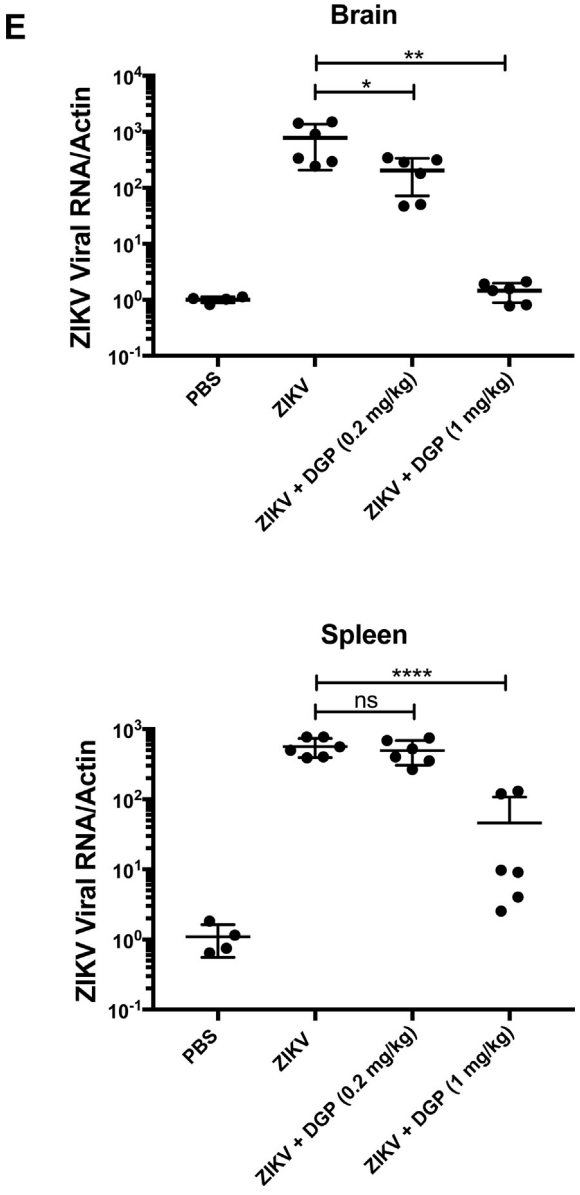

Fig. 5. DGP prevents ZIKV-induced mortality in type I Interferon receptor knockout mice (*Ifnar1*$^{-/-}$). C57BL/6 *Ifnar1*$^{-/-}$ mice were subcutaneously challenged (footpad) with 5 PFUs of the ZIKV strain MR766 in conjunction with the indicated amounts of DGP solubilized in PBS. Mortality (A,C) and body weight (B,D) were monitored daily for 15 days post-challenge. Mock challenges were performed using PBS alone. Each challenged group contained 6 mice, which were 3–4 week-old. Mice were weighed daily, excluding the day that they were found dead or sacrificed. Weights are expressed as percentage of body weight prior to infection, and standard deviations are shown. (E) Three independent groups of mice were challenged by injecting ZIKV(5 PFU) in conjunction with 0.2 mg/kg, or 1 mg/kg of DGP. As a control, mice were only injected with ZIKV(5 PFU). Mice were sacrificed 6 days post-infection and used to determine viral loads in brain (upper panel) and spleen (lower panel). Organs were lysed, and total RNA was extracted using TRIzol as described in Methods. Total RNA was used to determine the levels of ZIKV RNA by qRT-PCR using specific primers against ZIKV. Viral RNA levels were normalized to actin. Log-Rank (Mantel-Cox) test is shown.

fluorescence intensity (MFI) in Fig. 7B. These results suggested that DGP prevents the acidification of endosomes/lysosomes, which is required for the fusion of ZIKV [35,50–52], thus resulting in the inhibition of ZIKV infection.

4. Discussion

Our study has discovered that the natural compound DGP has the ability to potently inhibit ZIKV infection in human cell lines (*in vitro*) and in mice (*in vivo*). In addition, DGP shows broad-spectrum antiviral activity by blocking other *flaviviruses* such as DENV1, TBEV, WNV, and JEV. We also found that the active component of DGP is the diphyllin molecule, which, by itself, is less potent against ZIKV compared with DGP. Mechanistic studies revealed that DGP inhibits ZIKV infection at a pre-fusion step or during fusion of the virus. Our study also shows that DGP prevents the acidification of endosomes and therefore, inhibits the fusion of the viral membrane with the cellular membrane.

DGP inhibits ZIKV infection *in vitro* in different monkey and human cell lines without triggering cellular toxicity. Our results demonstrated that DGP concentrations in the nanomolar range [IC_{50} = 10–70 nM (0.01–0.07 μM)] inhibit ZIKV infection. In contrast, inhibition of ZIKV infection by chloroquine, a drug that also inhibits ZIKV fusion by preventing acidification of endosomes, requires concentrations in the micromolar range [35,50,66,67]. Based on our data, DGP is a better inhibitor when compared to Nanchangmycin, which inhibits ZIKV infection at an IC_{50} = ~100 − 400 nM [52]. Interestingly, Nanchangmycin, like DGP, also blocks viral entry, but not by preventing acidification of endosomes (data not shown). Recent observations have suggested that Nanchangmycin blocks viral internalization/endocytosis [68].

A combination of experiments allowed us to conclude that DGP inhibits ZIKV infection at a pre-fusion step or during fusion. *In situ* hybridization studies showed that DGP prevents the replication of viral RNA. The use of qRT-PCR to detect ZIKV RNA in cells treated with DGP confirmed the lack of viral RNA replication in these cells. Consistent with these results, we showed that DGP prevents the activation of the type I IFN response by ZIKV infection. Altogether, our results indicated that DGP prevents the entry of ZIKV contents into the host cytosol, suggesting that the DGP-induced block is at a pre-fusion step or during viral fusion.

DGP is a broad-spectrum antiviral that not only potently blocks ZIKV infection, but also inhibits infection by other *flaviviruses*. This makes DGP an ideal candidate for the clinical treatment of *flaviviruses*. However, despite blocking infection of every *flavivirus* tested in this work, DGP failed to block SeV infection, suggesting that the drug has a certain degree of specificity towards *flaviviruses*. In spite of its broad antiviral activity, DGP may still prove to be an effective anti-ZIKV drug, and may address the urgent need to combat new ZIKV infections in high-risk populations, infection of medical personnel in ZIKV affected areas, and prevent mother-to-child transmission of ZIKV.

Our results showed that DGP prevents ZIKV-induced mortality in the type I Interferon receptor knockout mice when the drug is co-injected with the virus, thus suggesting the potential of DGP to inhibit ZIKV infection *in vivo*. Our results implied that DGP inhibits ZIKV infection by preventing acidification of endosomes. Interestingly, the anti-malarial drugs chloroquine and the related hydroxychloroquine also block ZIKV infection *in vivo* and prevent acidification of endosomes. These drugs have been studied for its ability to inhibit mother-to-child transmission of ZIKV in mice [51,67]. Chloroquine and hydroxychloroquine are Food and Drug administration (FDA)-approved drugs to treat malaria, and they can also be used to treat ZIKV infections. However, the required inhibitory concentrations of these drugs for ZIKV in cell culture are in the micromolar range [50,66], unlike DGP, which is only required in the nanomolar concentration range. Also, *in vivo* experiments have shown that the required inhibitory concentration of Chloroquine is 50–100 mg/kg in mice [66]. Although more extensive testing of DGP *in vivo* is required, our results suggested that DGP might be effective against ZIKV infection at low concentrations *in vivo*. In addition to drugs that prevent acidification of endosomes, other compounds have been described to inhibit ZIKV *in vivo* [69]. For example, analogs such as BCX4430 [70], Sofosbuvir [71] or NITD008 [72] protected mice from ZIKV infection. Other compounds such as 25-hydroxycholesterol has also proven to reduced viremia and conferred protection against ZIKV in mice and rhesus macaques [73].

This work utilizes as an animal model of ZIKV infection, the type I interferon knockout mouse. All our infections were performed in 3–4

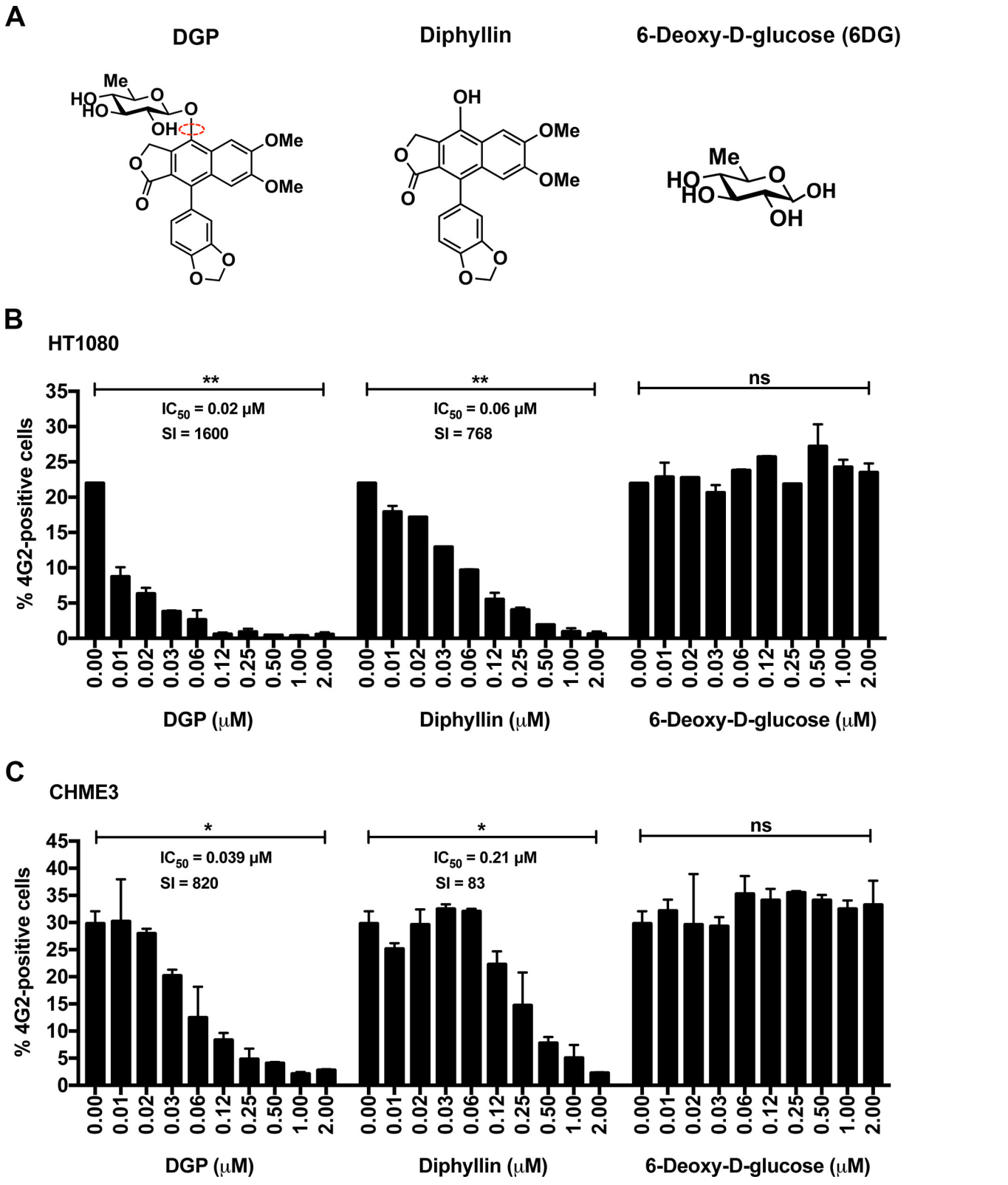

Fig. 6. The active component of DGP is diphyllin. (A) The molecular structures of DGP, diphyllin, and 6-Deoxy-D-Glucose are shown. (B) HT1080 or (C) CHME3 cells were infected with ZIKV MR766 at an MOI of 0.5 in the presence of increasing concentrations of the indicated molecules. At 48 h post-challenge, infection was determined by measuring the percentage 4G2-positive cells. The IC_{50} and selectivity index (SI) values are shown for each of the dose-dependent curves. The SI was calculated by the ratio of CC_{50} to IC_{50}. Experiments were performed at least three times and results of a representative experiment are shown. Bars represent the Mean ± SD. P < .05 (*), P < .01 (**), P < .001 (***), or not significant (ns), using two-tailed Student's *t*-test are shown.

weeks-old mice with ZIKV MR766, as shown in [18,21]. However, it has been reported that infection of 7–10 weeks-old mice by ZIKV MR766 does not lead to death [74].Overall these different results showed the limitations of our mouse model, and suggested that ZIKV-induced death depends on many factors such as mouse age, viral dose, and route of inoculation, as previously discussed [75]. Although the type I

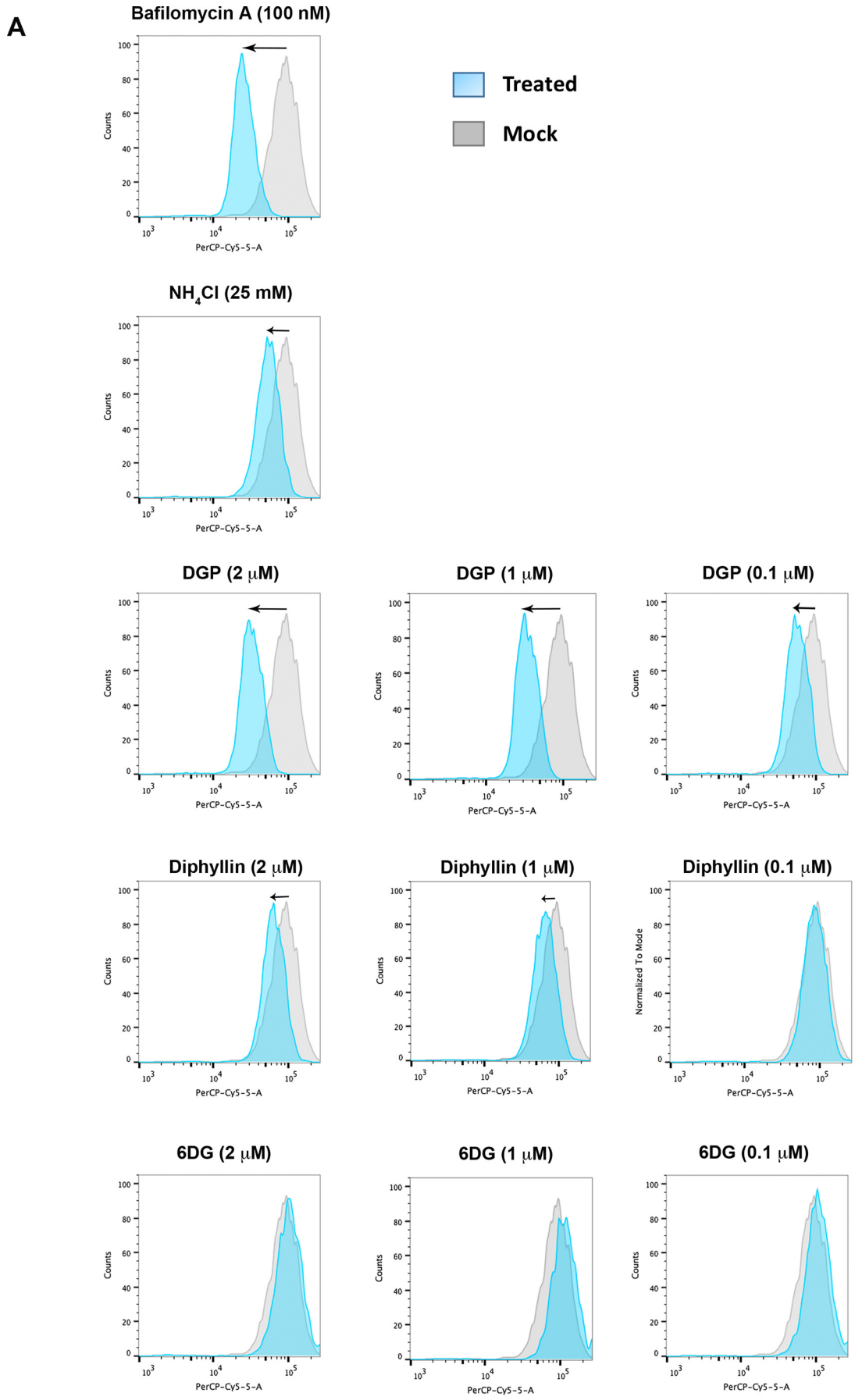
A
Bafilomycin A (100 nM)
Treated
Mock
NH4Cl (25 mM)
DGP (2 μM)
DGP (1 μM)
DGP (0.1 μM)
Diphyllin (2 μM)
Diphyllin (1 μM)
Diphyllin (0.1 μM)
6DG (2 μM)
6DG (1 μM)
6DG (0.1 μM)
Counts
Normalized To Mode
PerCP-Cy5-5-A

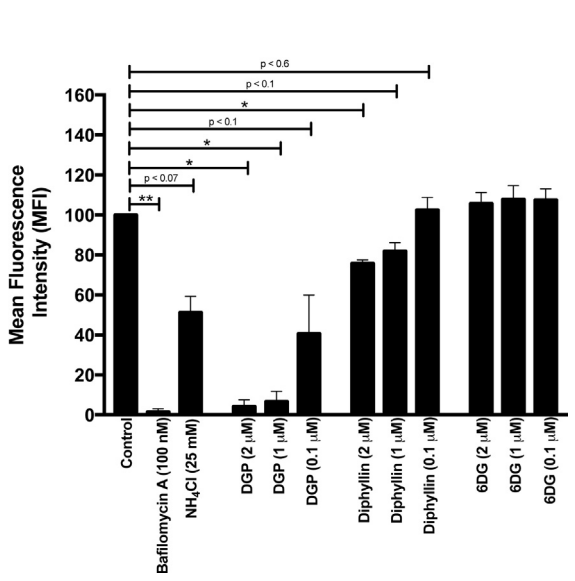

Fig. 7. DGP prevents acidification of endosomes. (A) Human HT1080 cells were treated with the indicated concentrations of DGP, diphyllin, or 6DG for 4 h. Subsequently, cells were incubated with 1 μg/mL acridine orange (AO) for 30 min. The fluorescence intensity of AO was measured by flow cytometry using the PerCP-Cy5–5-A (695 nm) channel. As controls, similar experiments were performed using Bafilomycin A1 and NH_4Cl. Changes in fluorescence are shown using histograms and the black arrow represents the shift in fluorescence of the total cell population. Experiments were performed at least three times, and results of a representative experiment are shown. (B) The loss of red fluorescence intensity compared with stained non-treated control cells (measured in the PerCP-Cy5–5-A channel) is represented as Mean Fluorescence Intensity (MFI). Bars representing the Mean ± SD. P < .05 (*), P < .01 (**), using two-tailed Student's *t*-test are shown.

interferon knockout mice has the limitation that is defective in innate antiviral responses [20], this mouse model is transnationally and clinically relevant due to the following features: 1) ZIKV infection of this mouse occurs in similar organs causing similar diseases when compared to humans (brain, testis, spleen, and the eye) [75], 2) ZIKV infection of this mouse reproduces the neurological symptoms observed in humans such as tremors, ataxia and paralysis [75], and 3) ZIKV infection of this mouse is reverted by the use of small molecules or antibodies against the virus supporting its relevance on evaluating vaccines and therapeutics [75]. Overall the type I interferon knockout mouse is a robust model to perform preclinical studies in the search of new therapies for ZIKV infection.

To investigate the part of the molecular structure of DGP responsible for the inhibition of ZIKV infection, we separately analyzed the two components of DGP, 6DG and Diphyllin. Our results showed that diphyllin is the active component of DGP, causing ZIKV inhibition. Interestingly, diphyllin was less potent than DGP, indicating that 6DG showed a small but measurable contribution towards DGP's ability to inhibit ZIKV infection. Studies have suggested that diphyllin has several cellular functions, as follows: 1) it inhibits vacuolar-ATPase activity [62,76]; 2) it inhibits endosomal acidification [63]; and 3) it inhibits topoisomerase IIa [31,32]. We and others have previously suggested that ZIKV infection is affected by inhibiting endosomal acidification [35,53–57]. In agreement with the literature, we showed that both diphyllin and DGP prevent endosome acidification to inhibit ZIKV infection. However, DGP is more potent in preventing endosomal acidification when compared with diphyllin, thus suggesting the additive effect of 6DG in DGDP-induced ZIKV inhibition. Overall, we have identified the inhibition mechanism of a novel compound DGP that blocks ZIKV infection both *in vitro* and *in vivo*.

Supplementary data to this article can be found online at https://doi.org/10.1016/j.ebiom.2019.08.060.

Funding sources

This work was supported by the Albert Einstein College of Medicine.

The funding sources played no role on the development of the research, preparation of manuscript, conclusions, and submission of manuscript.

Author contributions

A.M.L conducted the *in vitro* and *in vivo* experiments of ZIKV, virus production and infections. M.P conducted the RVP production and qRT-PCR experiments. M.P.C. and S.S. performed the (+)-ZIKV RNA hybridization staining. Z.H. and R.L. provided reagents. T.W. and S.L. performed the replicon experiments. A.M.L. and F.D.G. wrote the manuscript. F.D.G. design all the experiments.

Declaration of Competing Interest

The authors declare no competing interests.

Acknowledgments

We thank Dr. Paul Bates for the ZIKV strain MR766.

References

[1] Cao-Lormeau VM, Blake A, Mons S, Lastere S, Roche C, Vanhomwegen J, et al. Guillain-Barre syndrome outbreak associated with Zika virus infection in French Polynesia: a case-control study. Lancet 2016;387(10027):1531–9.
[2] Baud D, Gubler DJ, Schaub B, Lanteri MC, Musso D. An update on Zika virus infection. Lancet 2017;390(10107):2099–109.
[3] Parra B, Lizarazo J, Jimenez-Arango JA, Zea-Vera AF, Gonzalez-Manrique G, Vargas J, et al. Guillain-Barre syndrome associated with Zika virus infection in Colombia. N Engl J Med 2016;375(16):1513–23.
[4] Lazear HM, Diamond MS. Zika virus: new clinical syndromes and its emergence in the Western hemisphere. J Virol 2016;90(10):4864–75.
[5] Ramos da Silva S, Gao SJ. Zika virus: an update on epidemiology, pathology, molecular biology, and animal model. J Med Virol 2016;88(8):1291.
[6] Weaver SC, Costa F, Garcia-Blanco MA, Ko AI, Ribeiro GS, Saade G, et al. Zika virus: history, emergence, biology, and prospects for control. Antiviral Res 2016;130:69–80.
[7] Abushouk AI, Negida A, Ahmed H. An updated review of Zika virus. J Clin Virol 2016;84:53–8.
[8] Russell K, Hills SL, Oster AM, Porse CC, Danyluk G, Cone M, et al. Male-to-female sexual transmission of Zika virus-United States, January-April 2016. Clin Infect Dis 2017;64(2):211–3.
[9] Tang WW, Young MP, Mamidi A, Regla-Nava JA, Kim K, Shresta S. A mouse model of Zika virus sexual transmission and vaginal viral replication. Cell Rep 2016;17(12):3091–8.
[10] Cunha MS, Esposito DL, Rocco IM, Maeda AY, Vasami FG, Nogueira JS, et al. First complete genome sequence of Zika virus (Flaviviridae, Flavivirus) from an autochthonous transmission in Brazil. Genome Announc 2016;4(2).
[11] Ellison DW, Ladner JT, Buathong R, Alera MT, Wiley MR, Hermann L, et al. Complete genome sequences of Zika virus strains isolated from the blood of patients in Thailand in 2014 and the Philippines in 2012. Genome Announc 2016;4(3).
[12] Enfissi A, Codrington J, Roosblad J, Kazanji M, Rousset D. Zika virus genome from the Americas. Lancet 2016;387(10015):227–8.
[13] Giovanetti M, Faria NR, Nunes MRT, de Vasconcelos JM, Lourenco J, Rodrigues SG, et al. Zika virus complete genome from Salvador, Bahia, Brazil. Infect Genet Evol 2016;41:142–5.
[14] Ladner JT, Wiley MR, Prieto K, Yasuda CY, Nagle E, Kasper MR, et al. Complete genome sequences of five Zika virus isolates. Genome Announc 2016;4(3).
[15] Nandy A, Dey S, Basak SC, Bielinska-Waz D, Waz P. Characterizing the Zika virus genome - a bioinformatics study. Curr Comput Aided Drug Des 2016;12(2):87–97.
[16] Miner JJ, Cao B, Govero J, Smith AM, Fernandez E, Cabrera OH, et al. Zika virus infection during pregnancy in mice causes placental damage and fetal demise. Cell 2016;165(5):1081–91.
[17] Muthumani K, Griffin BD, Agarwal S, Kudchodkar SB, Reuschel EL, Choi H, et al. In vivo protection against ZIKV infection and pathogenesis through passive antibody transfer and active immunisation with a prMEnv DNA vaccine. NPJ Vaccines 2016;1:16021.
[18] Lazear HM, Govero J, Smith AM, Platt DJ, Fernandez E, Miner JJ, et al. A mouse model of Zika virus pathogenesis. Cell Host Microbe 2016;19(5):720–30.
[19] Muller U, Steinhoff U, Reis LF, Hemmi S, Pavlovic J, Zinkernagel RM, et al. Functional role of type I and type II interferons in antiviral defense. Science 1994;264(5167):1918–21.
[20] Bradfute SB, Warfield KL, Bray M. Mouse models for filovirus infections. Viruses 2012;4(9):1477–508.

[21] Tripathi S, Balasubramaniam VR, Brown JA, Mena I, Grant A, Bardina SV, et al. A novel Zika virus mouse model reveals strain specific differences in virus pathogenesis and host inflammatory immune responses. PLoS Pathog 2017;13(3):e1006258.
[22] Rossi SL, Tesh RB, Azar SR, Muruato AE, Hanley KA, Auguste AJ, et al. Characterization of a novel murine model to study Zika virus. Am J Trop Med Hyg 2016;94(6):1362–9.
[23] Dowall SD, Graham VA, Rayner E, Atkinson B, Hall G, Watson RJ, et al. A susceptible mouse model for Zika virus infection. PLoS Negl Trop Dis 2016;10(5):e0004658.
[24] Zmurko J, Marques RE, Schols D, Verbeken E, Kaptein SJ, Neyts J. The viral polymerase inhibitor 7-Deaza-2'-C-Methyladenosine is a potent inhibitor of in vitro Zika virus replication and delays disease progression in a robust mouse infection model. PLoS Negl Trop Dis 2016;10(5):e0004695.
[25] Smith DR, Hollidge B, Daye S, Zeng X, Blancett C, Kuszpit K, et al. Neuropathogenesis of Zika virus in a highly susceptible immunocompetent mouse model after antibody blockade of type I interferon. PLoS Negl Trop Dis 2017;11(1):e0005296.
[26] Elong Ngono A, Vizcarra EA, Tang WW, Sheets N, Joo Y, Kim K, et al. Mapping and role of the CD8(+) T cell response during primary Zika virus infection in mice. Cell Host Microbe 2017;21(1):35–46.
[27] Newman DJ, Cragg GM. Natural products as sources of new drugs from 1981 to 2014. J Nat Prod 2016;79(3):629–61.
[28] Zhang HJ, Rumschlag-Booms E, Guan YF, Wang DY, Liu KL, Li WF, et al. Potent inhibitor of drug-resistant HIV-1 strains identified from the medicinal plant Justicia gendarussa. J Nat Prod 2017;80(6):1798–807.
[29] Susplugas S, Hung NV, Bignon J, Thoison O, Kruczynski A, Sevenet T, et al. Cytotoxic arylnaphthalene lignans from a Vietnamese acanthaceae, Justicia patentiflora. J Nat Prod 2005;68(5):734–8.
[30] Makar S, Saha T, Singh SK. Naphthalene, a versatile platform in medicinal chemistry: sky-high perspective. Eur J Med Chem 2019;161:252–76.
[31] Shi DK, Zhang W, Ding N, Li M, Li YX. Design, synthesis and biological evaluation of novel glycosylated diphyllin derivatives as topoisomerase II inhibitors. Eur J Med Chem 2012;47(1):424–31.
[32] Zhao Y, Ni C, Zhang Y, Zhu L. Synthesis and bioevaluation of diphyllin glycosides as novel anticancer agents. Arch Pharm (Weinheim) 2012;345(8):622–8.
[33] Dick GW, Kitchen SF, Haddow AJ. Zika virus. I. Isolations and serological specificity. Trans R Soc Trop Med Hyg 1952;46(5):509–20.
[34] Liu S, DeLalio LJ, Isakson BE, Wang TT. AXL-mediated productive infection of human endothelial cells by Zika virus. Circ Res 2016;119(11):1183–9.
[35] Persaud M, Martinez-Lopez A, Buffone C, Porcelli SA, Diaz-Griffero F. Infection by Zika viruses requires the transmembrane protein AXL, endocytosis and low pH. Virology 2018;518:301–12.
[36] Stapleford KA, Moratorio G, Henningsson R, Chen R, Matheus S, Enfissi A, et al. Whole-genome sequencing analysis from the chikungunya virus Caribbean outbreak reveals novel evolutionary genomic elements. PLoS Negl Trop Dis 2016;10(1):e0004402.
[37] Mukherjee S, Pierson TC, Dowd KA. Pseudo-infectious reporter virus particles for measuring antibody-mediated neutralization and enhancement of dengue virus infection. Methods Mol Biol 2014;1138:75–97.
[38] Savidis G, McDougall WM, Meraner P, Perreira JM, Portmann JM, Trincucci G, et al. Identification of Zika virus and dengue virus dependency factors using functional genomics. Cell Rep 2016;16(1):232–46.
[39] Wagner AM, Loganbill JK, Besselsen DG. Detection of Sendai virus and pneumonia virus of mice by use of fluorogenic nuclease reverse transcriptase polymerase chain reaction analysis. Comp Med 2003;53(2):173–7.
[40] Wang F, Flanagan J, Su N, Wang LC, Bui S, Nielson A, et al. RNAscope: a novel in situ RNA analysis platform for formalin-fixed, paraffin-embedded tissues. J Mol Diagn 2012;14(1):22–9.
[41] Puray-Chavez M, Tedbury PR, Huber AD, Ukah OB, Yapo V, Liu D, et al. Multiplex single-cell visualization of nucleic acids and protein during HIV infection. Nat Commun 2017;8(1):1882.
[42] Thome MP, Filippi-Chiela EC, Villodre ES, Migliavaca CB, Onzi GR, Felipe KB, et al. Ratiometric analysis of Acridine Orange staining in the study of acidic organelles and autophagy. J Cell Sci 2016;129(24):4622–32.
[43] Kanzawa T, Germano IM, Komata T, Ito H, Kondo Y, Kondo S. Role of autophagy in temozolomide-induced cytotoxicity for malignant glioma cells. Cell Death Differ 2004;11(4):448–57.
[44] Garg TK, Chang JY. 15-deoxy-delta 12, 14-Prostaglandin J2 prevents reactive oxygen species generation and mitochondrial membrane depolarization induced by oxidative stress. BMC Pharmacol 2004;4:6.
[45] Balazs R, Jorgensen OS, Hack N. N-methyl-D-aspartate promotes the survival of cerebellar granule cells in culture. Neuroscience 1988;27(2):437–51.
[46] Hamel R, Dejarnac O, Wichit S, Ekchariyawat P, Neyret A, Luplertlop N, et al. Biology of Zika virus infection in human skin cells. J Virol 2015;89(17):8880–96.
[47] Meertens L, Labeau A, Dejarnac O, Cipriani S, Sinigaglia L, Bonnet-Madin L, et al. Axl mediates ZIKA virus entry in human glial cells and modulates innate immune responses. Cell Rep 2017;18(2):324–33.
[48] Kim JA, Seong RK, Son SW, Shin OS. Insights into ZIKV-mediated innate immune responses in human dermal fibroblasts and epidermal keratinocytes. J Invest Dermatol 2019;139(2):391–9.
[49] Martinez-Lopez A, Martin-Fernandez M, Buta S, Kim B, Bogunovic D, Diaz-Griffero F. SAMHD1 deficient human monocytes autonomously trigger type I interferon. Mol Immunol 2018;101:450–60.
[50] Delvecchio R, Higa LM, Pezzuto P, Valadao AL, Garcez PP, Monteiro FL, et al. Chloroquine, an endocytosis blocking agent, inhibits Zika virus infection in different cell models. Viruses 2016;8(12).
[51] Li C, Zhu X, Ji X, Quanquin N, Deng YQ, Tian M, et al. Chloroquine, a FDA-approved drug, prevents Zika virus infection and its associated congenital microcephaly in mice. EBioMedicine 2017;24:189–94.
[52] Rausch K, Hackett BA, Weinbren NL, Reeder SM, Sadovsky Y, Hunter CA, et al. Screening bioactives reveals Nanchangmycin as a broad Spectrum antiviral active against Zika virus. Cell Rep 2017;18(3):804–15.
[53] Gollins SW, Porterfield JS. pH-dependent fusion between the flavivirus West Nile and liposomal model membranes. J Gen Virol 1986;67:157–66 Pt 1.
[54] Randolph VB, Stollar V. Low pH-induced cell fusion in flavivirus-infected Aedes albopictus cell cultures. J Gen Virol 1990;71:1845–50 Pt 8.
[55] Smit JM, Moesker B, Rodenhuis-Zybert I, Wilschut J. Flavivirus cell entry and membrane fusion. Viruses 2011;3(2):160–71.
[56] Vorovitch MF, Timofeev AV, Atanadze SN, Tugizov SM, Kushch AA, Elbert LB. pH-dependent fusion of tick-borne encephalitis virus with artificial membranes. Arch Virol 1991;118(1–2):133–8.
[57] Pierson TC, Kielian M. Flaviviruses: braking the entering. Curr Opin Virol 2013;3(1):3–12.
[58] Chu JJ, Ng ML. Infectious entry of West Nile virus occurs through a clathrin-mediated endocytic pathway. J Virol 2004;78(19):10543–55.
[59] Bousse T, Takimoto T, Gorman WL, Takahashi T, Portner A. Regions on the hemagglutinin-neuraminidase proteins of human parainfluenza virus type-1 and Sendai virus important for membrane fusion. Virology 1994;204(2):506–14.
[60] Scheid A, Choppin PW. Identification of biological activities of paramyxovirus glycoproteins. Activation of cell fusion, hemolysis, and infectivity of proteolytic cleavage of an inactive precursor protein of Sendai virus. Virology 1974;57(2):475–90.
[61] Faisca P, Desmecht D. Sendai virus, the mouse parainfluenza type 1: a longstanding pathogen that remains up-to-date. Res Vet Sci 2007;82(1):115–25.
[62] Shen W, Zou X, Chen M, Liu P, Shen Y, Huang S, et al. Effects of diphyllin as a novel V-ATPase inhibitor on gastric adenocarcinoma. Eur J Pharmacol 2011;667(1–3):330–8.
[63] Sorensen MG, Henriksen K, Neutzsky-Wulff AV, Dziegiel MH, Karsdal MA. Diphyllin, a novel and naturally potent V-ATPase inhibitor, abrogates acidification of the osteoclastic resorption lacunae and bone resorption. J Bone Miner Res 2007;22(10):1640–8.
[64] Forgac M. Vacuolar ATPases: rotary proton pumps in physiology and pathophysiology. Nat Rev Mol Cell Biol 2007;8(11):917–29.
[65] Yoshimori T, Yamamoto A, Moriyama Y, Futai M, Tashiro Y. Bafilomycin A1, a specific inhibitor of vacuolar-type H(+)-ATPase, inhibits acidification and protein degradation in lysosomes of cultured cells. J Biol Chem 1991;266(26):17707–12.
[66] Shiryaev SA, Mesci P, Pinto A, Fernandes I, Sheets N, Shresta S, et al. Repurposing of the anti-malaria drug chloroquine for Zika virus treatment and prophylaxis. Sci Rep 2017;7(1):15771.
[67] Cao B, Parnell LA, Diamond MS, Mysorekar IU. Inhibition of autophagy limits vertical transmission of Zika virus in pregnant mice. J Exp Med 2017;214(8):2303–13.
[68] Hackett BA, Cherry S. Flavivirus internalization is regulated by a size-dependent endocytic pathway. Proc Natl Acad Sci U S A 2018;115(16):4246–51.
[69] Saiz JC, Martin-Acebes MA. The race to find antivirals for Zika virus. Antimicrob Agents Chemother 2017;61(6).
[70] Julander JG, Siddharthan V, Evans J, Taylor R, Tolbert K, Apuli C, et al. Efficacy of the broad-spectrum antiviral compound BCX4430 against Zika virus in cell culture and in a mouse model. Antiviral Res 2017;137:14–22.
[71] Bullard-Feibelman KM, Govero J, Zhu Z, Salazar V, Veselinovic M, Diamond MS, et al. The FDA-approved drug sofosbuvir inhibits Zika virus infection. Antiviral Res 2017;137:134–40.
[72] Deng YQ, Zhang NN, Li CF, Tian M, Hao JN, Xie XP, et al. Adenosine analog NITD008 is a potent inhibitor of Zika virus. Open Forum Infect Dis 2016;3(4):ofw175.
[73] Li C, Deng YQ, Wang S, Ma F, Aliyari R, Huang XY, et al. 25-hydroxycholesterol protects host against Zika virus infection and its associated microcephaly in a mouse model. Immunity 2017;46(3):446–56.
[74] Carbaugh DL, Baric RS, Lazear HM. Envelope protein glycosylation mediates Zika virus pathogenesis. J Virol 2019;93(12).
[75] Morrison TE, Diamond MS. Animal models of Zika virus infection, pathogenesis, and immunity. J Virol 2017;91:8.
[76] Chen H, Liu P, Zhang T, Gao Y, Zhang Y, Shen X, et al. Effects of diphyllin as a novel V-ATPase inhibitor on TE-1 and ECA-109 cells. Oncol Rep 2018;39(3):921–8.